Enhanced Coercivity in Co-Rich Near-Stoichiometric $Co_xFe_{3-x}O_{4+\delta}$ Nanoparticles Prepared in Large Batches

German Salazar-Alvarez,*[,†,‡] Richard T. Olsson,[§] Jordi Sort,[||,#] Waldemar A. A. Macedo,[⊥] José D. Ardisson,[⊥] Maria Dolors Baró,[||] Ulf W. Gedde,[§] and Josep Nogués[‡,#]

Department of Materials Science and Engineering and Fibre and Polymer Technology, Royal Institute of Technology, SE-100 44 Stockholm, Sweden, Institut Català de Nanotecnologia, Campus Universitat Autònoma de Barcelona, E-08193 Bellaterra, Spain, Institució Catalana de Recerca i Estudis Avançats (ICREA), Spain, Departament de Física, Universitat Autònoma de Barcelona, E-08193 Bellaterra, Spain, and Laboratório de Física Aplicada, Centro de Desenvolvimento da Tecnologia Nuclear, 30123-970 Belo Horizonte, Minais Gerais, Brazil

Received March 26, 2007. Revised Manuscript Received June 13, 2007

The relationship between the structure and composition with the magnetic properties of near stoichiometric cobalt ferrite nanoparticles $Co_xFe_{3-x}O_{4+\delta}$ ($0.85 < x < 1.1$) prepared in large batches with average sizes in the range 60−210 nm has been investigated. Chemical analysis and Rietveld refinement of the X-ray diffraction data in conjunction with Mössbauer spectroscopy allowed us to identify an interplay between particle size, microstructure (concentration of interstitial ions, microstrain, cation arrangement in octahedral and tetrahedral sites), and composition, which sensitively controls the magnetic properties such as coercivity and saturation magnetization. In all cases, cobalt-rich compositions resulted in a higher coercivity, whereas lower degrees of inversion and higher iron contents led to slightly higher saturation magnetization values.

1. Introduction

Magnetic nanoparticles have drawn a lot of attention the past decade because of their complex fundamental properties (e.g., superparamagnetism, surface anisotropy, or exchange bias) and their widespread applications ranging from in vivo target drug delivery and ferrofluids to high-frequency magnetoelectric devices and high-density recording media.[1−8] Ferrite nanoparticles of the type MFe_2O_4 (where M is a divalent ion) have been studied because of their attractive functional properties, e.g., large resistivities, or tunable magnetic properties and low cost.[8,9] Cobalt ferrite ($CoFe_2O_4$) particles were extensively investigated during the 1980s because of their rather large anisotropy and their potential application as magnetic recording media.[10] Recently, Co−ferrite nanoparticles have gained renewed interest because of the appealing novel magnetic properties such as photo-induced magnetic effects,[11] doping or strain enhanced coercivity,[12−14] the so-called multiferroic materials,[15] and their catalytic properties.[16] However, systematic studies of $Co_xFe_{3-x}O_{4+\delta}$ nanoparticles have mostly been limited to particles synthesized by "dry organic-based chemistry". The dry chemistry approaches allow for fine-tuning of the composition and microstructural parameters,[17] but the very small yield of the reactions make this process unpractical for industrial purposes. The low-cost wet-chemistry approach (e.g., aqueous precipitation methods) is more versatile and the most likely method to be used in large-scale production of magnetic nanoparticles for applied science.[18]

* Corresponding author: e-mail: gsa.icn@gmail.com.
† Department of Materials Science and Engineering, Royal Institute of Technology.
‡ Institut Català de Nanotecnologia.
§ Fibre and Polymer Technology, Royal Institute of Technology.
|| Departament de Fìsica, Universitat Autònoma de Barcelona.
Institució Catalana de Recerca i Estudis Avançats (ICREA).
⊥ Centro de Desenvolvimento da Tecnologia Nuclear.

(1) Hyeon, T. *Chem. Commun.* **2003**, 927.
(2) Willard, M. A.; Kurihara, L. K.; Carpenter, E. E.; Calvin, S.; Harris, V. G. *Int. Mater. Rev.* **2004**, *49*, 125.
(3) (a) Tartaj, P.; Morales, M. P.; Veintemillas-Verdaguer, S.; González-Carreño, T.; Serna, C. J. *J. Phys. D* **2003**, *36*, R182. (b) Pankhurst, Q. A.; Connolly, J.; Jones, S. K.; Dobson, J. *J. Phys. D* **2003**, *36*, R167.
(4) Batlle, X.; Labarta, A. *J. Phys. D* **2002,** *35*, R15.
(5) Gubin, S. P.; Koksharov, Y. A.; Khomutov, G. B.; Yurkov, G. Y. *Russ. Chem. Rev.* **2005**, *74*, 489.
(6) Nogués, J.; Sort, J.; Langlais, V.; Skumryev, V.; Suriñach, S.; Muñoz, J. S.; Baró, M. D. *Phys. Rep.* **2005**, *422*, 65.
(7) Morrison, S. A.; Cahill, C. L.; Carpenter, E. E.; Calvin, S.; Harris, V. G. *J. Nanosci. Nanotechnol.* **2005**, *5*, 1323.
(8) Vestal, C. R.; Zhang, Z. J. *Int. J. Nanotechnol.* **2004,** *1*, 240.
(9) Park, J.; An, K.; Hwang, Y.; Park, J. G.; Noh, H. J.; Kim, J. Y.; Park, J. H.; Hwang, N. M.; Hyeon, T. *Nat. Mater.* **2004**, *3*, 891.
(10) Sharrock, M. P. *IEEE Trans. Magn.* **1989**, *25*, 4374.
(11) Giri, A. K.; Kirkpatrick, E. M.; Moongkhamklang, P.; Majetich, S. A.; Harris, V. G. *Appl. Phys. Lett.* **2002,** *80*, 2341.
(12) Ding, J.; Chen, Y. J.; Shi, Y.; Wang, S. *Appl. Phys. Lett.* **2000,** *77*, 3621.
(13) Liu, B. H.; Ding, J.; Dong, Z. L.; Boothroyd, C. B.; Yin, J. H.; Yi, J. B. *Phys. Rev. B* **2006**, *74*, 184427.
(14) Liu, B. H.; Ding, J. *Appl. Phys. Lett.* **2006**, *88*, 042506.
(15) Zheng, H.; Wang, J.; Lofland, S. E.; Ma, Z.; Mohaddes-Ardabili, L.; Zhao, T.; Salamanca-Riba, L.; Shinde, S. R.; Ogale, S. B.; Bai, F.; Viehland, D.; Jia, Y.; Schlom, D. G.; Wuttig, M.; Roytburd, A.; Ramesh, R. *Science* **2004**, *303*, 661.
(16) Manova, E.; Tsoncheva, T.; Estournes, C.; Paneva, D.; Tenchev, K.; Mitov, I.; Petrov, L. *Appl. Catal. A* **2006,** *300*, 170.
(17) (a) Hyeon, T.; Chung, Y.; Park, J.; Lee, S. S.; Kim, Y. W.; Park, B. H. *J. Phys. Chem. B* **2002**, *106*, 6831. (b) Sun, S.; Zeng, H.; Robinson, D. B.; Raoux, S.; Rice, P. R.; Wang, S. X.; Li, G. *J. Am. Chem. Soc.* **2004**, *126*, 273.
(18) (a) Sugimoto, T., Ed. *Fine Particles: Synthesis, Characterization, and Mechanisms of Growth*; Marcel Dekker: New York, 2000; Vol. 92. (b) Cushing, B. L.; Kolesnichenko, V. L.; O'Connor, C. J. *Chem. Rev.* **2004**, *104*, 3893.

10.1021/cm070827t CCC: $37.00
Published on Web 09/08/2007

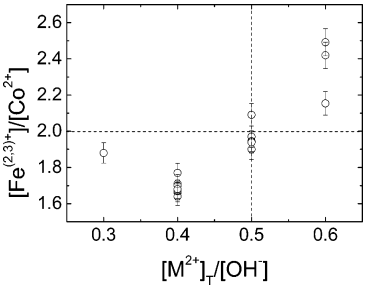

Figure 1. Variation of the cobalt concentration with the synthesis ratio $[M^{2+}]_T/[OH^-]$.[23] The dashed lines indicate the stoichiometric values.

From a structural standpoint, the formula unit of stoichiometric ferrites can be written as $(M_yFe_{1-y})[M_{1-y}Fe_{1+y}]O_4$, where the round brackets denote tetrahedral sites (A), the squared brackets represent octahedral sites [B], and the inversion degree is defined as $\Delta \equiv 1 - y$. The distribution of cations in the different positions (A) and [B], i.e., the chemical order, as well as deviation from the ideal 1:2 ratio (M:Fe) are known to affect their magnetic properties.[19−21] However, reports of the effects of small deviations from the ideal stoichiometric composition for Co−ferrite nanoparticles are very scarce,[22] even though the impact of these deviations on the magnetic properties is very significant.

Previously,[23] we reported on the chemical conditions to synthesize large batches of well-defined ferrites powders (>16 g/batch) with compositions close to the stoichiometric using the wet chemistry approach. The chemical composition, $[Fe^{(2,3)+}]/[Co^{2+}]$, and the density of the particles, ρ, varied between $0.85 < x < 1.1$, and $4400 < \rho < 5100$ kg/m^3, respectively. In this article, we present the correlation between the structural/morphological characteristics (i.e., chemical order, non-stoichiometry, particle size, occupancy ratio, cation distribution) and the magnetic properties of $Co_xFe_{3-x}O_{4+\delta}$ nanoparticles with $0.85 < x < 1.1$ prepared in large batches. The magnetic properties were found to be very sensitive to the different structural parameters and in particular to the Co content, which, in turn, could be directly controlled by careful adjustment of the synthesis conditions.

2. Experimental Section

2.1. Synthesis. The synthesis of the particles has been described in detail in a previous publication.[23] Briefly, an aqueous solution of iron(II) sulfate and cobalt(II) chloride with a constant stoichiometric ratio of 2 was heated to 90 °C and quickly added to a 2 dm^3 three-neck round-bottom flask containing an aqueous solution of sodium hydroxide and potassium nitrate, as mild oxidizing reagent,[24] under mechanical stirring at 90 °C. The final molar ratio of total metal ions to hydroxide ions, $([Fe^{2+}]+[Co^{2+}])/[OH^-] = [M^{2+}]_T/[OH^-]$, was varied from 0.3 to 0.6. The reaction mixture was maintained at the above-mentioned temperature for 3 h, after which the particles were separated using a hard magnet and washed thoroughly with water.

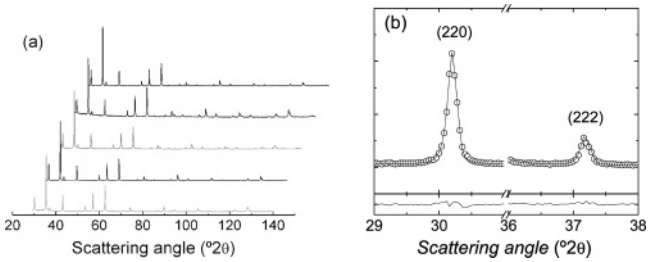

Figure 2. (a) XRD patterns of samples corresponding to various $[M^{2+}]_T/[OH^-]$ ratios (from top to bottom, 0.30, 0.40, 0.53, 0.57, and 0.60). (b) Magnified view corresponding to the reflections of the (220) and (222) planes of a sample with $[M^{2+}]_T/[OH^-] = 0.57$; the graph below corresponds to the difference between the experimental profile and the calculated one. The symbols represent the experimental data, whereas the lines are fits using the Rietveld method (see text for more details).

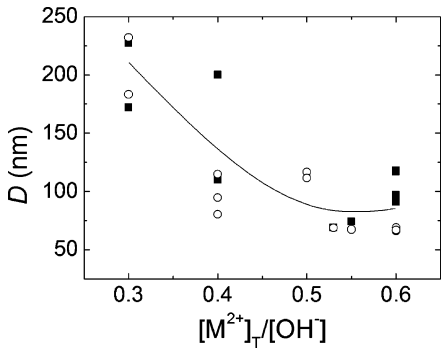

Figure 3. Variation of the mean crystallite diameter, D_X, (open circles) and the volume-weighted physical diameter, D^v_P, (full squares) with the metal to hydroxide $[M^{2+}]_T/[OH^-]$ ratio. The solid line is a guide to the eye.

2.2. Characterization Techniques. The concentration of cobalt and iron in the precipitated nanoparticles was determined by atomic absorption spectroscopy (AAS, Perkin-Elmer). The microstructure of the particles was characterized by X-ray diffraction (XRD) using a Philips 3050 diffractometer with CuK_α radiation ($\lambda = 0.154021$ nm) in the range 30−140° and a scan rate of 0.004 °/s. Analysis of the XRD data was undertaken with a full-pattern fitting procedure based on the Rietveld method.[25] Hysteresis loops of the powders were recorded in an Oxford Instruments vibrating sample magnetometer (VSM) at room temperature using a maximum applied field of 11 kOe. Mössbauer spectra were obtained at 90 K using a conventional constant acceleration transmission setup and a ^{57}Co/Rh source. Velocity calibration was done using a 12 μm foil of metallic iron (α-Fe), and the Mössbauer parameters are given relative to this standard at room temperature. Low-resolution transmission electron micrographs (TEM) were obtained in a Tecnai 10 apparatus operating at 100 kV. High-resolution transmission electron micrographs (HRTEM) were taken in a JEOL 2010 electron microscope using an accelerating voltage of 200 kV.

3. Results

A number of samples were prepared under different synthesis ratios, $[M^{2+}]_T/[OH^-]$. The composition, x, calcu-

(19) Hamdeh, H. H.; Ho, J. C.; Oliver, S. A.; Willey, R. J.; Olivieri, G.; Busca, G. *J. Appl. Phys.* **1997,** *81*, 1851.
(20) Lüders, U.; Bibes, M.; Bobo, J. F.; Cantoni, M.; Bertacco, R.; Fontcuberta, J. *Phys. Rev. B* **2005**, *71*, 134419.
(21) Smit, J.; Wijn, H. P. J. *Ferrites: Physical Properties of Ferri-magnetic Oxides in Relation to Their Technical Applications*; Philips: Endhoven, The Netherlands, 1959.
(22) (a) Li, X.; Kutal, C. *J. Alloys Compd.* **2003**, *349*, 264. (b) Franco Júnior, A.; de Oliveira Lima, E. C.; Novak, M. A.; Wells, P. R., Jr. *J. Magn. Magn. Mater.* **2007**, *308*, 198. (c) Na, J. G.; Lee, T. D.; Park, S. J. *IEEE Trans. Magn.* **1992**, *28*, 2433.
(23) Olsson, R. T.; Salazar-Alvarez, G.; Hedenqvist, M. S.; Gedde, U. W.; Lindberg, F.; Savage, S. *Chem. Mater.* **2005**, *17*, 5109.
(24) (a) Sugimoto, T.; Matijevic, E. *J. Colloid Interface Sci.* **1980**, *74*, 227. (b) Tamura, H.; Matijević, E. *J. Colloid Interface Sci.* **1982**, *90*, 100.
(25) (a) Rietveld, H. M. *Acta Crystallogr.* **1966**, *20*, 508. (b) Young, R. A. *The Rietveld Method*; Oxford University Press: Oxford, U.K., 1995. (c) Lutterotti, L.; Gialanella, S. *Acta Mater.* **1997**, *46*, 101.

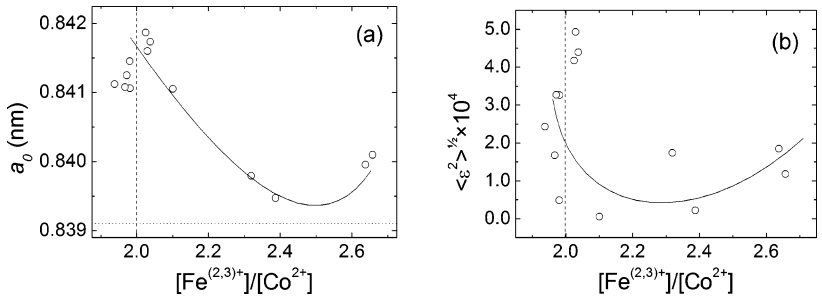

Figure 4. Variation of (a) lattice cell parameter, a_0, and (b) microstrain, $<\epsilon^2>^{1/2}$, with the composition ratio. The continuous lines are added as a guide to the eye; the dotted line shows the bulk value of a_0, whereas the dashed lines indicate the stoichiometric value $[Fe^{(2,3)+}]/[Co^{2+}] = 2$.

lated from the metal molar ratio, $[Fe^{(2,3)+}]/[Co^{2+}]$, assuming the stoichiometry of the compound as $Co_xFe_{3-x}O_{4+\delta}$, varied between $0.85 < x < 1.1$, i.e., $1.7 < [Fe^{(2,3)+}]/[Co^{2+}] < 2.5$ when varying the $[M^{2+}]_T/[OH^-]$ in the 0.3−0.6 range. As can be seen in Figure 1, the cobalt content increased from a substoichiometric composition ($x < 1$) to a superstoichiometric composition ($x > 1$) when increasing the $[M^{2+}]_T/[OH^-]$ synthesis ratio, in good agreement with earlier studies.[24b]

3.1. Microstructural Studies. The XRD patterns acquired for samples prepared under different synthesis ratios, $[M^{2+}]_T/[OH^-]$, are shown in Figure 2. The patterns were index-matched with those ones corresponding to $CoFe_2O_4$ (JCPDS card 22-1086) and no secondary crystalline phases were observed. The peaks from the diffractograms were fitted with a pseudo-Voigt function to determine the Lorentzian component (related to particle size effects) and the Gaussian component (related to microstrain). Figure 3 shows the range of particle (crystallite) sizes determined from the XRD fits, D_X, as a function of the $[Fe^{(2,3)+}]/[Co^{2+}]$ ratio. The figure shows that the particle size decreases as the $[Fe^{(2,3)+}]/[Co^{2+}]$ and $[M^{2+}]_T/[OH^-]$ ratios increase. As expected, the particle size becomes smaller when the concentration of the metal salt is increased, because it leads to a higher number of nucleation sites and a lower concentration of monomers available for the subsequent particle growth. Note that the particle sizes tend to stabilize (around 80 nm) near the stoichiometric point at $[M^{2+}]_T/[OH^-] \approx 0.5$, in agreement with earlier reports.[23,24]

The cell parameter, a_0, decreased by increasing the $[Fe^{(2,3)+}]/[Co^{2+}]$ ratio stabilizing toward the bulk value of cobalt ferrite (JCPDS card 22-1086), as shown in Figure 4a. Because decreasing the synthesis ratio results in a higher cobalt content in the particles, the observed increment of the lattice cell parameter at low $[Fe^{(2,3)+}]/[Co^{2+}]$ ratios can be expected to be due to an excess of Co(II) ions in the crystal unit cell, whereas the increment at high $[Fe^{(2,3)+}]/[Co^{2+}]$ ratios may result in an excess of iron species. Another plausible explanation would be the formation of interstitial ions. Such variations would affect the crystal lattice parameter and also the average microstrain, $<\epsilon^2>^{1/2}$. Figure 4b shows the nonmonotonic variation of the microstrain with the metal composition ratio $[Fe^{(2,3)+}]/[Co^{2+}]$ displaying a minimum for compositions near the stoichiometric value.

The analysis of the XRD diffractograms yielded also information on the overall cation arrangement in the spinel structure. For instance, it is known that in the case of spinels,

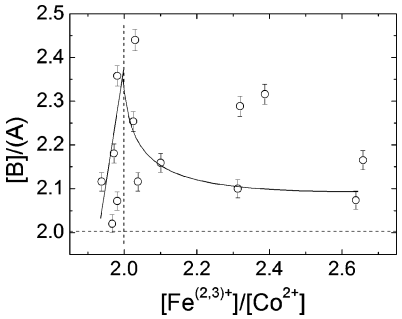

Figure 5. Variation of the occupancy ratio [B]/(A) with the composition ratio $[Fe^{(2,3)+}]/[Co^{2+}]$. The continuous lines are added as a guide to the eye and the dashed lines indicate the stoichiometric values.

the intensity of the (220) reflection, $I^{(220)}$, is due only to the concentration of ions in tetrahedral positions, (a), whereas the intensity of the (222) reflection, $I^{(222)}$, is related only to the concentration of ions in octahedral positions (denoted as [B]).[26] Hence, the intensity ratio $I^{(222)}/I^{(220)}$ provides us with information on the different occupancy ratio, [B]/(A), of the metal ions in the spinel structure (see fittings in Figure 2b). To obtain the [B]/(A) ratios, the occupancy of the tetrahedral and octahedral positions was set as a refinable parameter at the final stages of the fitting. Note that because the atomic scattering factors and absorption coefficients for Fe and Co are rather similar (within 5%), they were assumed to change equally. Figure 5 shows the variation of the occupancy ratio [B]/(A) with the composition ratio. From the values reported in the figure it can be seen that the octahedral occupancy, [B], increases steeply close for Co-rich compositions ($[Fe^{(2,3)+}]/[Co^{2+}] < 2$) to decrease monotonically toward a cobalt-deficient compositions ($[Fe^{(2,3)+}]/[Co^{2+}] > 2$).

The composition and crystallinity were further assessed with high-resolution electron microscopy. For example, Figure 6 shows the analysis carried out on a sample with a $[Fe^{(2,3)+}]/[Co^{2+}] = 2.3$. Figure 6(a) shows a selected area electron diffraction (SAED) with the diffraction rings index-matched to those of spinel cobalt ferrite (JCPDS card 22-1086). Figure 6(b) evidence the lattice planes corresponding to the (111) reflections of the spinel phase[27] crossing the whole particle, demonstrating the single-crystalline character of the nanoparticles.

Transmission electron microscopy was also used to evaluate the particle size and the size distribution of the different

(26) Šepelák, V.; Baabe, D.; Mienert, D.; Schultze, D.; Krumeich, F.; Litterst, F. J.; Becker, K. D. *J. Magn. Magn. Mater.* **2003**, *257*, 377.
(27) Cornell, R. M.; Schwertmann, U. *The Iron Oxides*, 2nd ed.; Wiley-VCH: Weinheim, Germany, 2003.

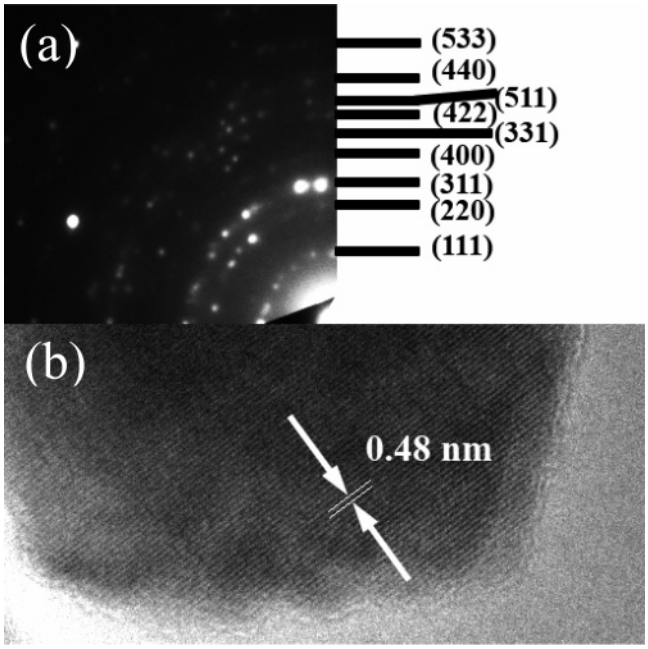

Figure 6. (a) SAED and (b) HRTEM image of particles with a $[Fe^{(2,3)+}]/[Co^{2+}] = 2.3$. The rings of the diffraction pattern are index-matched with those of $CoFe_2O_4$ (JCPDS card 22-1086). The lattice fringe of 0.48 nm corresponds to the interplanar distance of the (111) reflections.

samples. Images a and b of Figure 7 present the results for samples prepared with $[M^{2+}]_T/[OH^-]$ ratios of 0.4 and 0.6, respectively. Because of the volume dependence of the magnetic properties and the XRD, the particle size distributions are presented as volume-weighted distributions. The distributions show that the particles prepared at low synthesis ratios are rather polydispersed, whereas those prepared at high synthesis ratios have a relative narrower size distribution, as can be seen in panels c and d of Figure 7, respectively. The volume weight size average, D^v_P, for the different samples is given in Figure 3, along with that obtained from the diffractograms. Both averages obtained for particles prepared at $[M^{2+}]_T/[OH^-] < 0.6$ agree fairly well. However, the volume weight average size for particles obtained at $[M^{2+}]_T/[OH^-] = 0.6$ are larger than the corresponding D_X. Such apparent disagreement could be intrinsic to the volume distribution since the particles are counted by hand and large particles are easily oversampled.[28]

3.2. Magnetic Characterization. Some of the hysteresis loops recorded for the powders are shown in Figure 8a, whereas panels b and c in Figure 8 display the variation of saturation magnetization, M_S, and the coercivity, H_C, of the nanoparticles with the chemical composition, $[Fe^{(2,3)+}]/[Co^{2+}]$. Figure 8b shows that the saturation magnetization of the samples decreases as the content of cobalt increases. From Figure 8c, it can be observed that the coercivity of the particles with a cobalt-rich composition, $H_C \approx 1.5$ kOe, is notably larger than the one for stoichiometric compositions, decreasing, to stabilize near $H_C = 0.85$ kOe, for the cobalt-deficient particles.

Because of the variation of particle sizes shown in Figure 3, it is important to discern the diverse variables affecting the magnetic properties of the samples. Figure 9 shows the variation of the coercivity as a function of the particle size, D_X. The coercivity increases with the particle size over a wide range of sizes, from ca. 60 nm toward >200 nm. This trend is opposite to what would be expected from critical single domain size of Co−ferrite, $D_{Crit} \approx 40-80$ nm.[29,30] Namely, for $<D> > D_{Crit}$, one would expect H_C to decrease with increasing crystallite size as the system enters into the multidomain region. Another possible factor influencing the magnetic properties would be the stress anisotropy[13,14] due to the large magnetostriction of $CoFe_2O_4$ ($\lambda_S \approx -260 \times 10^{-6}$),[31] because the different particles exhibit diverse microstrain values. However, given the large size of the nanoparticles, the microstrains are exceedingly small to significantly affect the coercivity.

4. Discussion

In a previous report,[23] it has been shown that there is a clear correlation between the synthesis ratio $[M^{2+}]_T/[OH^-]$ and the final composition ratio $[Fe^{(2,3)+}]/[Co^{2+}]$. Actually, the variation of the composition ratio, $[Fe^{(2,3)+}]/[Co^{2+}]$, can be achieved by varying $[M^{2+}]_T/[OH^-]$ even while using a constant ratio $[Fe^{(2,3)+}]/[Co^{2+}] = 2$ throughout the syntheses, which has been proposed to arise from different rates of formation of the metal hydroxide precursors.

Therefore, varying the $[M^{2+}]_T/[OH^-]$ ratio away from the stoichiometric point resulted in the existence of (a) an excess of Co(II) ions at a low $[M^{2+}]_T/[OH^-]$ ratio and (b) the presence of hydroxyl ions at high $[M^{2+}]_T/[OH^-]$ ratio. Both of these conditions would increase the lattice cell parameter a_0, because the former would result in an excess of Co(II) ions in the unit cell combined with the possible formation of interstitial ions, whereas the latter would be due to the presence of the sterically hindered hydroxyl ion. Furthermore, the increment of interstitial metallic ions at low $[Fe^{(2,3)+}]/[Co^{2+}]$ and the existence of hydroxyl ions at high $[Fe^{(2,3)+}]/[Co^{2+}]$ would not only have an effect on the crystal lattice parameter but also on the average microstrain, $<\epsilon^2>^{1/2}$. Indeed, Figure 4b shows a non-monotonic behavior of $<\epsilon^2>^{1/2}$, similar to that of the lattice parameter presenting a minimum for compositions near the stoichiometric value. It has been argued that low $[M^{2+}]_T/[OH^-]$ ratios (condition to obtain $[Fe^{(2,3)+}]/[Co^{2+}] < 2$) produced fewer Fe(II) ions than high $[M^{2+}]_T/[OH^-]$ ratios. This is due to the excess of hydroxyl ions needed to catalyze the oxidation of Fe(II) by nitrate ions.[24] Hence, the opposite condition, i.e., a high $[M^{2+}]_T/[OH^-]$, would preserve more Fe(II) in solution during the formation of the spinel phase. Because Fe(II) is a larger cation than both Co(II) and Fe(III), it is expected that it will have higher preference for octahedral sites rather than the smaller tetrahedral cavities, which are preferred by the Fe(III) cations. It is expected that by the end of the reaction, all of the Fe(II) ions would have oxidized to Fe(III). Thus,

(28) Allen, T. *Particle Size Measurements*, 5th ed.; Chapman & Hall: London, 1997; Vol. 1.

(29) Berkowitz, A. E.; Schuele, W. J. *J. Appl. Phys.* **1959**, *30*, S134.

(30) Chinnasamy, C. N.; Jeyadevan, B.; Shinoda, K.; Tohji, K.; Djayaprawira, D. J.; Takahashi, M.; Justin Joseyphus, R.; Narayanasamy, A. *Appl. Phys. Lett.* **2003**, *83*, 2862.

(31) McCallum, R. W.; Dennis, K. W.; Jiles, D. C.; Snyder, J. E.; Chen, Y. H. *Low Temp. Phys.* **2001**, *27*, 266.

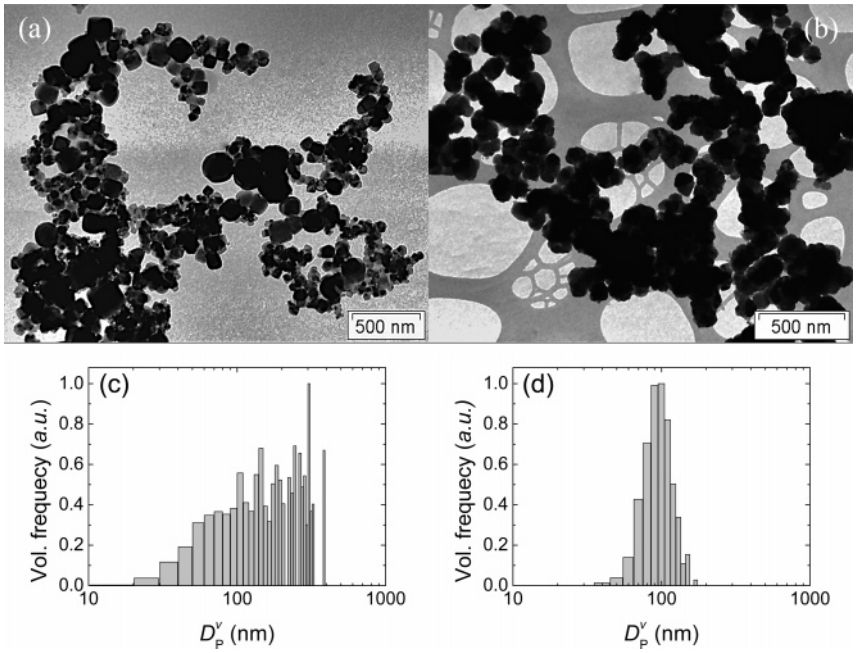

Figure 7. Low-resolution TEM images of samples prepared with a $[M^{2+}]_T/[OH^-]$ ratio of (a) 0.4 and (b) 0.6; (c,d) corresponding volume-weighted particle size distributions. Note the different magnification used for the TEM images.

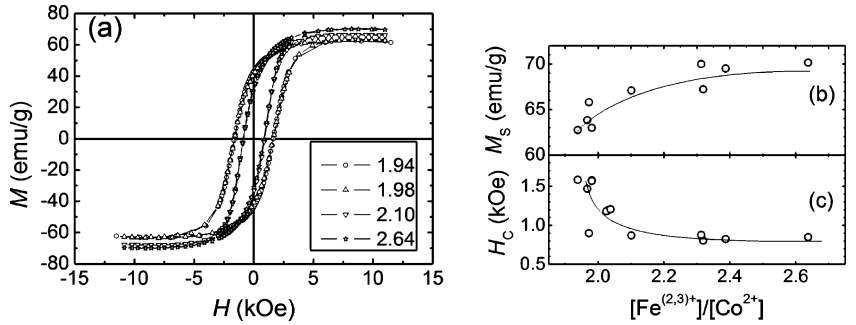

Figure 8. (a) Magnetic hysteresis loops of particles prepared with different composition ratios $[Fe^{(2,3)+}]/[Co^{2+}]$ and (b) variation of saturation magnetization, M_S, and (c) coercivity, H_C, of the materials with the chemical composition. The lines in (b) and (c) are guides to the eye.

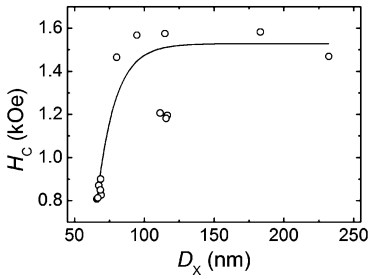

Figure 9. Variation of the coercivity, H_C, with the mean particle diameter, D_X.

the concentration of ions in tetrahedral sites would increase, and the occupancy ratio [B]/(A) would consequently decrease, behavior shown by the cobalt-lean samples in Figure 5. The overall high values of [B]/(A) > 2 and the lattice cell parameter a_0 > 0.8392 nm for all the samples could be due to a larger concentration of cations in octahedral positions arising from an incomplete migration of ions during the dehydration of the precursor.[32]

From the magnetic point of view, the increase of Fe(III) ions in tetrahedral places would explain the larger magnetization at high $[Fe^{(2,3)+}]/[Co^{2+}]$ ratios shown in Figure 8b.

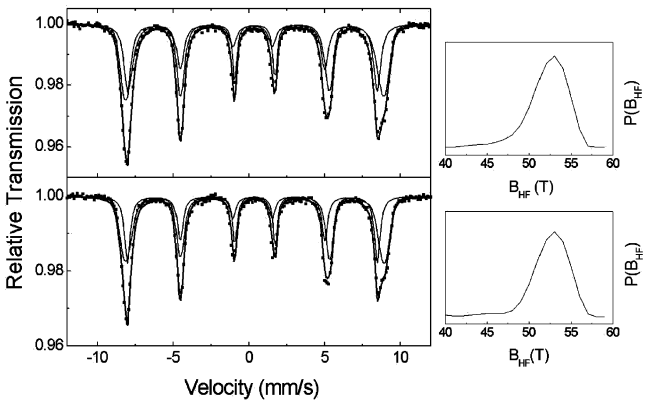

Figure 10. Mössbauer spectra obtained at 90 K for samples with (top) $[Fe^{(2,3)+}]/[Co^{2+}] = 1.94$ and (bottom) $[Fe^{(2,3)+}]/[Co^{2+}] = 2.38$. The symbols correspond to the measurement, whereas the sharp sextets correspond to the (A) sites, the broad ones (magnetic hyperfine field distributions, $P(B_{HF})$, shown at the right) to the [B] sites, and the thick solid line to the overall sum.

However, traditional analysis of M_S in ferrites is carried out assuming a formula unit of $(Co_yFe_{1-y})[Co_{1-y}Fe_{1+y}]O_4$ with Fe^{3+} and Co^{2+} having a magnetic moment of 5 μ_B and 3 μ_B, respectively. The analysis becomes more complex considering the non-stoichiometry of the occupancy ratio [B]/(A), the chemical composition $[Fe^{(2,3)+}]/[Co^{2+}]$ and the possible

(32) Cudennec, Y.; Lecerf, A. *Solid State Sci.* **2005**, *7*, 520.

Table 1. Mössbauer Parameters (line width Γ, isomer shift δ, quadrupole splitting Δ, magnetic hyperfine field B_{HF}, and relative area A at 90 K) of $Co_xFe_{3-x}O_{4+\delta}$ Nanoparticles

	(A)					[B][a]			
sample	Γ (mm/s)	δ (mm/s)	Δ (mm/s)	B_{HF} (kOe)	A (%)	δ (mm/s)	Δ (mm/s)	B_{HF} (kOe)	A (%)
S1	0.44	0.33	−0.00	511	38	0.50		527	62
S2	0.53	0.31	0.02	510	42	0.50		520	58
S3	0.56	0.33	0.03	511	41	0.48		525	59
S4	0.50	0.34	0.01	510	41	0.50		523	59
S5	0.55	0.34	−0.02	511	42	0.50		528	55
S6	0.54	0.35	−0.02	512	45	0.50		524	55
S7	0.48	0.33	−0.01	512	41	0.50		528	59
S8	0.44	0.34	−0.00	511	38	0.50		527	62
S9	0.57	0.36	−0.00	509	43	0.51		515	57

[a] Average value for δ and B_{HF}

Table 2. Formula Unit Composition and Degree of Inversion, Δ, of Some of the $Co_xFe_{3-x}O_{4+\delta}$ Samples, as Estimated from the Chemical Analysis, Mössbauer Spectra and Occupancy Ratio.

sample	$[Fe^{(2,3)+}]/[Co^{2+}]$	$Fe^{[B]}/Fe^{(A)}$	[B]/(A)	composition	degree of inversion, Δ
S1	2.66	1.66	2.17	$(Fe_{0.82}Co_{0.13})[Fe_{1.36}Co_{0.69}]O_{4+\delta}$	0.82
S2	2.32	1.46	2.29	$(Fe_{0.85}Co_{0.06})[Fe_{1.24}Co_{0.84}]O_{4+\delta}$	0.85
S3	2.39	1.46	2.32	$(Fe_{0.86}Co_{0.04})[Fe_{1.25}Co_{0.84}]O_{4+\delta}$	0.86
S4	2.03	1.26	2.25	$(Fe_{0.87}Co_{0.05})[Fe_{1.13}Co_{0.94}]O_{4+\delta}$	0.87
S5	2.03	1.35	2.44	$(Fe_{0.90}Co_{0.00})[Fe_{1.11}Co_{1.02}]O_{4+\delta}$	0.90
S6	2.04	1.29	2.12	$(Fe_{0.81}Co_{0.15})[Fe_{1.20}Co_{0.84}]O_{4+\delta}$	0.81
S7	1.98	1.48	2.36	$(Fe_{0.80}Co_{0.09})[Fe_{1.19}Co_{0.92}]O_{4+\delta}$	0.80
S8	1.94	1.63	2.12	$(Fe_{0.75}Co_{0.21})[Fe_{1.23}Co_{0.81}]O_{4+\delta}$	0.75
S9	1.96	1.31	2.01	$(Fe_{0.86}Co_{0.14})[Fe_{1.13}Co_{0.87}]O_{4+\delta}$	0.86

presence of Fe(II). Therefore, a more accurate composition of cobalt ferrites prepared in aqueous media would be given by a formula unit composition of $(Co_yFe^{III}_{1-z-u}Fe^{II}_u)[Co_{x-y}Fe^{II}_vFe^{III}_{2-x+z-v}]O_{4+\delta}$ with the inversion parameter defined as $\Delta = 1 - z - u$.

To better understand the behavior of the $Co_xFe_{3-x}O_{4+\delta}$ nanoparticles, we carried out Mössbauer spectroscopy on selected samples. Shown in Figure 10 are the spectra for samples with a $[Fe^{(2,3)+}]/[Co^{2+}] = 1.94$ and 2.38 with the corresponding fits, which because of the strong line overlapping were carried out assuming one sextet for the (A) site and a distribution of magnetic hyperfine fields, B_{HF}, for site [B] because the hyperfine parameters of the (A) sites are very insensitive to the Co content, whereas those at [B] sites are affected by the different nearest-neighbor occupancy at the tetrahedral (A) sites.[33] The main results from the Mössbauer study are summarized in Table 1. It can be seen that the B_{HF} for the (A) site is ∼511 kOe, whereas the distribution of B_{HF} for the [B] gives an average B_{HF} of ∼525 kOe. These results are consistent with literature B_{HF} values for cobalt ferrite nanoparticles and evidence a significant absence of Fe(II) species.[33]

Analysis of the hyperfine data provides with information on the distribution of Fe ions in octahedral and tetrahedral sites, i.e., the iron distribution ratio $Fe^{[B]}/Fe^{(A)}$. From the results of the chemical composition, the occupancy ratio, and the iron distribution ratio, it was possible to obtain an estimated composition of the samples as shown in Table 2 (more details are given in the Supporting Information). From the results, it can be readily seen that the Co^{2+} ions are found both in the (A) and [B] sites with a tendency to increased inversion (more Co^{2+} in the (A) sites) as the $[Fe^{(2,3)+}]/[Co^{2+}]$ ratio becomes smaller (larger *x*). As can be seen in Figure 8c, the samples with superstoichiometric concentration of Co^{2+} tend to have larger coercivity, H_C. However, for stoichiometric and substoichiometric cobalt concentrations other effects such as the amount of Co^{2+} in [B], the particle size and its distribution, the [B]/(A) ratio, a_0, or the microstrains can also play a role. The large coercivity in bulk stoichiometric $CoFe_2O_4$ has been traditionally explained by the single-ion anisotropy model,[34] arising from the contribution of the orbital magnetism of Co^{2+} ions at the [B] sites.[35−37] Namely, when the Co^{2+} ions migrate from the octahedral sites to the tetrahedral ones because of the variations in inversion produced by the synthesis conditions or annealing, the coercivity decreases because of the less anisotropic environment of the tetrahedral sites. However, for non-stoichiometric Co-ferrites, the situation can be more complex. In particular, for large Co^{2+} contents, the amount of Co^{2+} in octahedral sites could remain roughly constant, thus this contribution to the coercivity enhancement would be unchanged. However, as more Co^{2+} is introduced, it goes

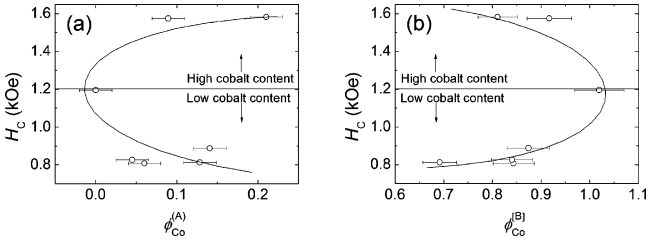

Figure 11. Variation of the coercivity, H_C, with the fraction of cobalt ions in (a) tetrahedral sites, $\phi^{(A)}_{Co}$, and (b) octahedral sites, $\phi^{[B]}_{Co}$, obtained from chemical analysis, XRD diffraction, and Mössbauer data.

(33) (a) Sawatzky, G. A.; van der Woude, F.; Morrish, A. H. *Phys. Rev.* **1969**, *187*, 747. (b) Sawatzky, G. A.; van der Woude, F.; Morrish, A. H. *J. Appl. Phys.* **1968**, *39*, 1204. (c) Dormann, J. L.; Greneche, J. L.; Pourroy, G.; Läkamp, S. *Hyperfine Interact.* **1998**, *112*, 89. (d) Lelis, M. F. F.; Porto, A. O.; Gonçalves, C. M.; Fabris, J. D. *J. Magn. Magn. Mater.* **2004**, *278*, 263.
(34) Berkowitz, A. E.; Schuele, W. J.; Flanders, P. J. *J. Appl. Phys.* **1968**, *39*, 1261.
(35) Slonczewski, J. C. *Phys. Rev.* **1958**, *110*, 1341.
(36) Wolf, W. P. *Phys. Rev.* **1957**, *108*, 1152.
(37) Song, Q., Zhang, Z. J. *J. Phys. Chem. B* **2006**, *110*, 11205.

into the tetrahedral or interstitial sites. Because Co^{2+} is more anisotropic than both Fe^{2+} and Fe^{3+}, having more Co^{2+} would still increase the overall anisotropy. Moreover, the presence of both Fe^{2+} and Fe^{3+} makes the quantitative analysis not straight forward, because these kinds of effects have not been studied systematically in controlled bulk materials. However, this trend should hold only for x values in $Co_xFe_{3-x}O_{4+\delta}$ close to the stoichiometric $CoFe_2O_4$ ($x \approx 1$), because Co_2FeO_4, i.e., $x \approx 2$, is only weakly anisotropic at room temperature because of the presence of low-spin Co^{3+} ions.[38,39]

It is clear from the structural and Mössbauer data that it becomes difficult to control one parameter at a time. Namely, by varying the $[M^{2+}]_T/[OH^-]$ ratio in the synthesis, not only does the $[Fe^{(2,3)+}]/[Co^{2+}]$ ratio change, as intended, but also the a_0, $<D>$, $<\epsilon^2>^{1/2}$, [B]/(A) ratio, and the amount of Co^{2+} in the (A) and [B] sites. Concomitantly, the magnetic properties are affected to different degrees by the diverse structural parameters. In general, as-obtained nanoparticles are likely to have [B]/(A) ratios away from the ideal inverse spinel ([B]/(A) = 2) of bulk $CoFe_2O_4$, which should depend on the synthesis method. Similarly, the exact $[Fe^{(2,3)+}]/[Co^{2+}]$ stoichiometry may be difficult to control in certain chemical processes. Both of these parameters, together with the amount of Co^{2+} in the (A) or [B] sites (also complex to control during the synthesis), strongly affect the properties of the Co−ferrite nanoparticles. Moreover, the magnetic properties of Co−ferrite nanoparticles could also be affected by the oxygen stoichiometry, which is known to modify the properties in bulk ferrites.[40] Consequently, this combination of effects makes the detailed correlation between the structural and magnetic results rather complex and actually may explain the spread of magnetic properties of Co−ferrite nanoparticles reported in the literature.[8−11,14,16,17,19−23,29−31,33] Nevertheless, there is a clear correlation between, for instance, high coercivity with larger overall Co^{2+} content and lower M_S with higher Co content.

5. Conclusions

In conclusion, we have shown that in the synthesis of off-stoichiometric Co-ferrite by a wet chemical route, several of the final structural parameters are strongly correlated, making it complicated to control one property at a time. The magnetic results indicate that excess of Co in the $Co_xFe_{3-x}O_{4+\delta}$ (with $x \approx 1$) may be an alternative route for the improvement of the coercivity of these ferrites.

Acknowledgment. The authors thank V. Langlais for her help during the early stages of this study. The work was financed by Spanish CICYT (MAT2007-66302-C02) and MEC (CSD2006-00012 Consolider-Ingenio 2010), the Catalan DGR (2005-SGR-00401), the Swedish Defence Research Agency (FOI), and the Brazilian MCT/CNPq. The authors thank the Serveis de Microscòpia and d'Anàlisi Química at UAB for their technical assistance. G.S.A. acknowledges the financial support provided by the KTH Rektors gåvomedel and the Institut Català de Nanotecnologia.

Supporting Information Available: Details on the determination of the particle composition based on the three different ratios obtained by independent techniques. This material is available free of charge via the Internet at http://pubs.acs.org.

CM070827T

(38) Smith, P. A.; Spencer, C. D.; Stillwell, R. P. *J. Phys. Chem. Solids* **1978**, *39*, 107.
(39) Kawano, S.; Achiwa, N. *Mater. Res. Bull.* **1976**, *11*, 911.
(40) Bonsdorf, G.; Schäffer, K.; Teske, K.; Langbein, H.; Ullman, H. *Solid State Ionics* **1998**, *110*, 73.